

Fig. 3. Ferroelectric hysteresis loops of  $(\text{NH}_4)_3\text{H}(\text{SO}_4)_2$ . (a) in Phase VII ( $p=5.6$  kbar,  $T=-86.6^\circ\text{C}$ ), (b) in Phase VI ( $p=5.6$  kbar,  $T=-56.5^\circ\text{C}$ ). Frequency: 50 Hz.

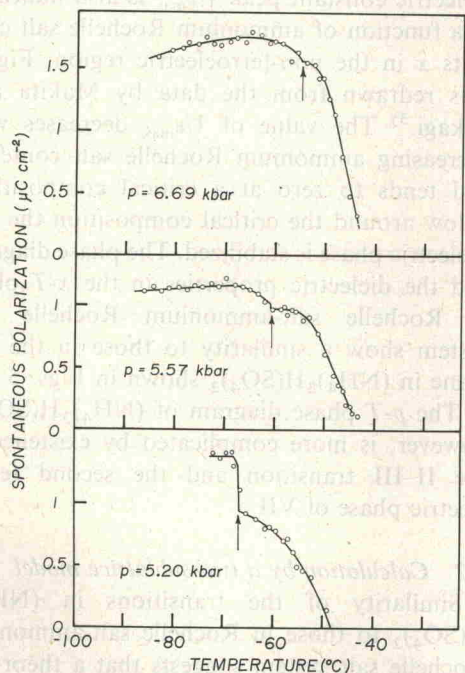


Fig. 4. Temperature dependence of the spontaneous polarization of  $(\text{NH}_4)_3\text{H}(\text{SO}_4)_2$  at different pressures. On heating process. The vertical arrows indicate the VII-VI transition.

the vertical arrows in Fig. 4. The discontinuity becomes unclear with increasing pressure; this is consistent with the diminution in the thermal hysteresis of transition.

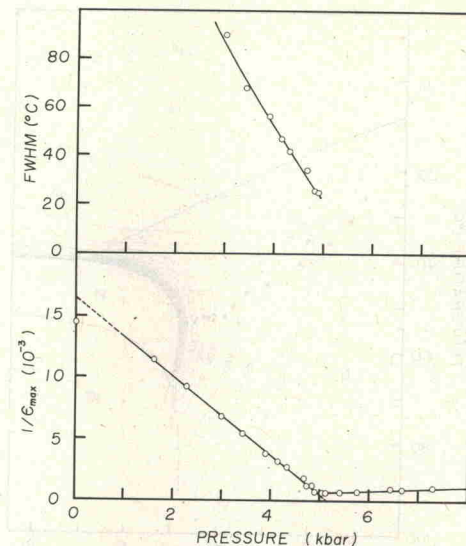


Fig. 5. Hydrostatic pressure dependence of the full width at half maximum (FWHM) of the broad peak of dielectric constant (above) and the inverse of the maximum value of dielectric constant (below) along the  $c^*$ -direction of  $(\text{NH}_4)_3\text{H}(\text{SO}_4)_2$ . In the below figure the inverse of the dielectric constant at the upper Curie point is plotted for the pressure region above 5 kbar.

Figure 5 shows the pressure dependence of the inverse of the maximum dielectric constant and of the full width at half maximum (FWHM) of the broad dielectric constant peak. Above about 1 kbar, the inverse of the maximum dielectric constant  $1/\epsilon_{\text{max}}$  linearly decreases with increasing pressure as  $1/\epsilon_{\text{max}} = C^*(p_0 - p)$ . The parameters are determined as  $C^* = (3.20 \pm 0.03) \times 10^{-3} \text{ kbar}^{-1}$  and  $p_0 = 5.1 \pm 0.1$  kbar. The ferroelectric VI Phase is stabilized above 5.0 kbar; slightly below the critical pressure  $p_0$ . In Fig. 5, above 5 kbar the inverse of the maximum dielectric constant at the upper Curie point (the III-VI or II-VI transition point) is plotted. The value of  $1/\epsilon_{\text{max}}$  slightly increases with increasing pressure in this pressure region. The full width at half maximum (FWHM) of the broad dielectric constant peak which is more than  $100^\circ\text{C}$  at 0 kbar rapidly decreases with increasing pressure as seen in Fig. 5.

Figure 6 indicates the pressure-temperature phase diagram below room temperature. In the figure the solid circles indicate the peak positions of the dielectric constant observed in constant pressure measurements. Contour lines of equal dielectric constant are indicated by

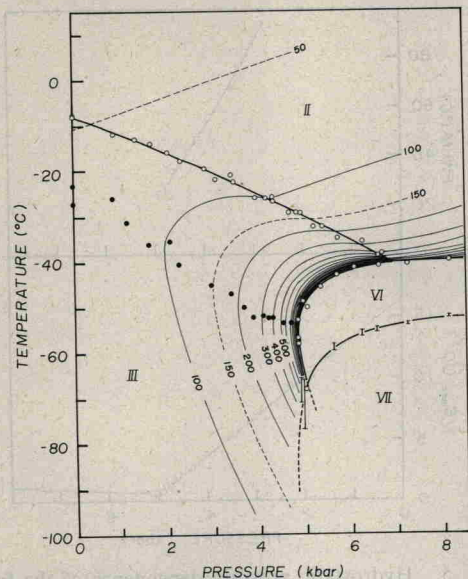


Fig. 6. Pressure-temperature phase diagram of  $(\text{NH}_4)_3\text{H}(\text{SO}_4)_2$  below room temperature. Open circles and vertical short bars indicate observed transition points. Solid circles indicate the maximum positions of the broad peak of the dielectric constant along the  $c^*$ -direction at  $p=\text{constant}$  measurements. Contour lines of equal dielectric constant are shown in Phases II and III.

thin curves for the non-ferroelectric phases of II and III. It is noted that a ridge of the dielectric constant extends in a direction roughly parallel to the II-III phase boundary. It is evident that the solid circles should be on the trajectory of contact points of contour curves and  $p=\text{constant}$  lines.

#### §4. Discussion

##### 4.1 Comparison with the Rochelle salt-ammonium Rochelle salt system

The results shown in Fig. 6 indicate that the polarization fluctuation which brings about the high pressure VI Phase is described in the two dimensional pressure-temperature space. Similar situation was already reported for Rochelle salt-ammonium Rochelle salt system by Makita and Takagi.<sup>5)</sup> As the contents of ammonium Rochelle salt decrease from about 15 at. % a broad peak of dielectric constant becomes more and more conspicuous, and below about 2.5 at. % of ammonium Rochelle salt contents the peak of dielectric constant splits into double maxima stabilizing a ferroelectric phase between them.

Figure 7 shows the phase diagram of Rochelle

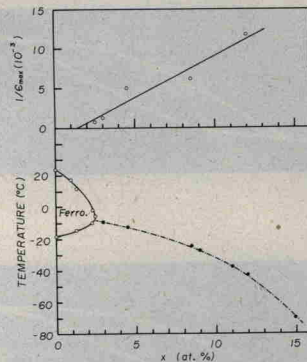


Fig. 7. Phase diagram of the Rochelle salt-ammonium Rochelle salt system (below) and the ammonium Rochelle salt content  $x$  dependence of the inverse of the maximum dielectric constant (above). In the below figure the position of the maximum dielectric constant in the non-ferroelectric phase is indicated by solid circles.

salt-ammonium Rochelle salt system. The inverse of the maximum value at the broad dielectric constant peak  $1/\epsilon_{\text{max}}$  is also indicated as a function of ammonium Rochelle salt contents  $x$  in the non-ferroelectric region. Figure 7 is redrawn from the data by Makita and Takagi.<sup>5)</sup> The value of  $1/\epsilon_{\text{max}}$  decreases with decreasing ammonium Rochelle salt contents, and tends to zero at a critical composition. Below around the critical composition the ferroelectric phase is stabilized. The phase diagram and the dielectric properties in the  $x$ - $T$  plane of Rochelle salt-ammonium Rochelle salt system show a similarity to those in the  $p$ - $T$  plane in  $(\text{NH}_4)_3\text{H}(\text{SO}_4)_2$  shown in Figs. 5 and 6. The  $p$ - $T$  phase diagram of  $(\text{NH}_4)_3\text{H}(\text{SO}_4)_2$ , however, is more complicated by existence of the II-III transition and the second ferroelectric phase of VII.

##### 4.2 Calculation by a two-sublattice model

Similarity of the transitions in  $(\text{NH}_4)_3\text{H}(\text{SO}_4)_2$  to those in Rochelle salt-ammonium Rochelle salt system suggests that a theory of Rochelle salt-type ferroelectrics may also be applied to  $(\text{NH}_4)_3\text{H}(\text{SO}_4)_2$ . In this section, Mitsui's two-sublattice model of Rochelle salt<sup>4)</sup> is modified to apply to a free crystal and is tried to apply to the problem of the phase transitions in  $(\text{NH}_4)_3\text{H}(\text{SO}_4)_2$ . Recent structural analysis showed that the non-ferroelectric II Phase allows an antiferroelectric arrangement of dipoles. Also a long-period